nature portfolio

https://doi.org/10.1038/s41586-026-10444-4

Supplementary information

A brain reward circuit inhibited by next-generation weight-loss drugs in mice

In the format provided by the authors and unedited

A Brain Reward Circuit Inhibited By Next-Generation Weight Loss Drugs in Mice

Authors

Elizabeth N. Godschall[1†], Taha Bugra Gungul[1†], Isabelle R. Sajonia[1†], Aleyna K. Buyukaksakal[1], Orien Dong-Ang Li[1], Sophia Ogilvie[1], Austin B. Keeler[1], Guilian Tian[2], Yu Shi[1], Omar Koita[3,4], Xinzhu Guo[1], Tyler C. J. Deutsch[5,6], Eric J. Steacy[5,7], Maisie Crook[1], YuChen Zhang[7], Nicholas J. Conley[1,7], Gulsun Memi[1,8], Addison N. Webster[1,7], O. Yipkin Calhan[1], Weile Liu[1], Amani Akkoub[1], Karan Malik[1], Kaleigh I. West[1], Sara Michel-Le[1], Arun Karthikeyan[1], Grace van Gerven[1], Olivia A. Dell'Aglio[1], Kevin T. Beier[2], Larry S. Zweifel[3,4], Manoj K. Patel[5,7], John N. Campbell[1,7,9], Christopher D. Deppmann[1,7, 9-11]*, Ali D. Güler[1,7,9]*

[1]Department of Biology, University of Virginia; Charlottesville, VA 22904, USA.
[2]Department of Physiology and Biophysics, University of California, Irvine; Irvine, CA, 92617, USA
[3]Department of Pharmacology, University of Washington; Seattle, WA, 98195, USA
[4]Department of Psychiatry, University of Washington; Seattle, WA, 98195, USA
[5]Department of Anesthesiology, University of Virginia; Charlottesville, VA 22904, USA.
[6]Edward Via College of Osteopathic Medicine; Blacksburg, VA, 24060, USA
[7]Neuroscience Graduate Program, University of Virginia; Charlottesville, VA 22903, USA.
[8]Department of Physiology, School of Medicine, Adiyaman University; Adiyaman 02040, Turkey.
[9]Program in Fundamental Neuroscience, University of Virginia; Charlottesville, VA 22904, USA.
[10]Department of Cell Biology, University of Virginia; Charlottesville, VA 22904, USA.
[11]Department of Biomedical Engineering, University of Virginia; Charlottesville, VA 22904, USA.

*Corresponding author. Email: deppmann@virginia.edu and aguler@virginia.edu.

†These authors contributed equally to this work.

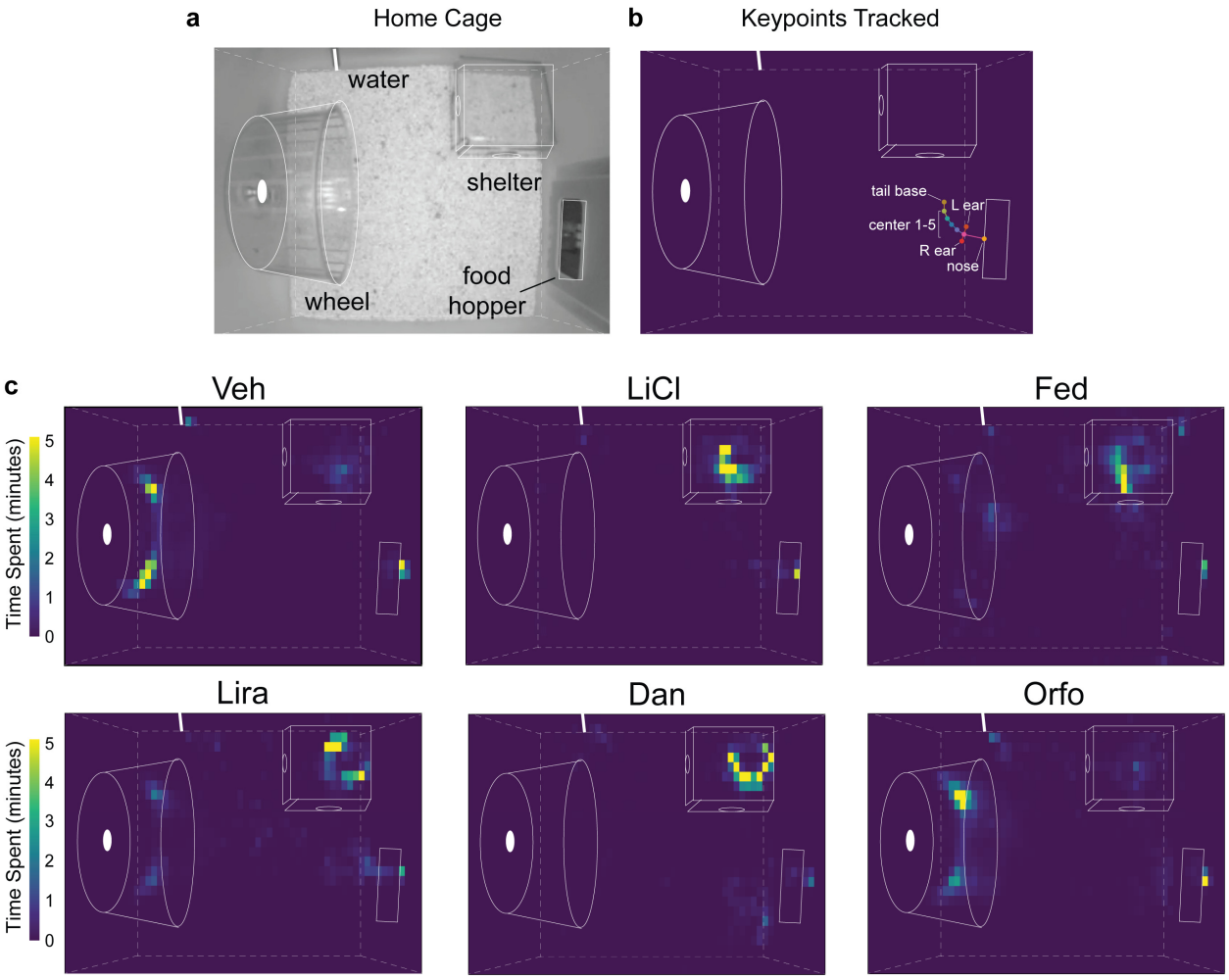

Supplemental Data Fig. 1. Home cage monitoring heatmaps of Glp1r^{S33W} mice. (**a**), Representative image of home cage set-up (dimensions: 30 x 30 x 43.5 cm) with bedding, showing calibrated positions of wheel, IR translucent shelter (10.5 x 10.5 x 6 cm), food hopper (5.5 cm from floor), and water bottle spout (5 cm from floor) identified in white outline (top). Videos were recorded using a top-down greyscale video recording system. (**b**) 9 Keypoints tracked on mice using SLEAP: nose, ears (L/R), tail base, and five body center points. (**c**), Coordinate-based heatmaps of nose keypoint trajectories recorded at 25 fps over 2-hour sessions for each treatment (ZT 12-14). Color scale represents dwelling time in minutes.

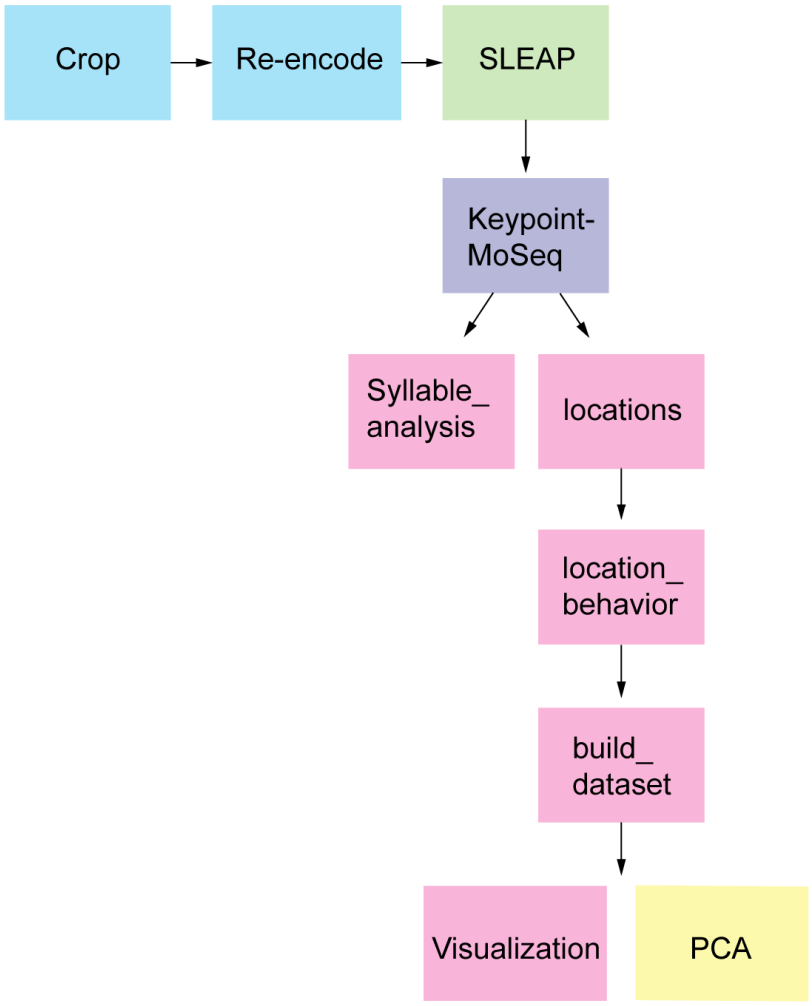

Supplemental Data Fig. 2. Machine-learning assisted behavioral analysis pipeline. Blue squares represent video pre-processing steps. Social LEAP Estimates Animal Poses (SLEAP) was used to extract nine keypoint coordinates for each mouse in the videos (**Fig. 2b-c, Supplemental Data Fig. 1b-c**). Keypoint Motion Sequencing (Keypoint-MoSeq) identified behavioral syllables from these coordinates (**Fig. 2d-f, Extended Data Figures 3-4, Supplemental Data Figures 3-4**). Pink squares represent Python scripts and the yellow square represents R scripts used for the analysis of Keypoint-MoSeq results: syllable-level analysis (**Fig. 2d-f, Extended Data Figures 3-4, Supplemental Data Fig. 4**), locations (identify regions of interest), location_behavior (**Fig. 2g-y**), build_dataset, Visualization (**Fig. 2g, 2s-x**), and PCA (**Fig. 2y, Extended Data Fig. 6y-z**).

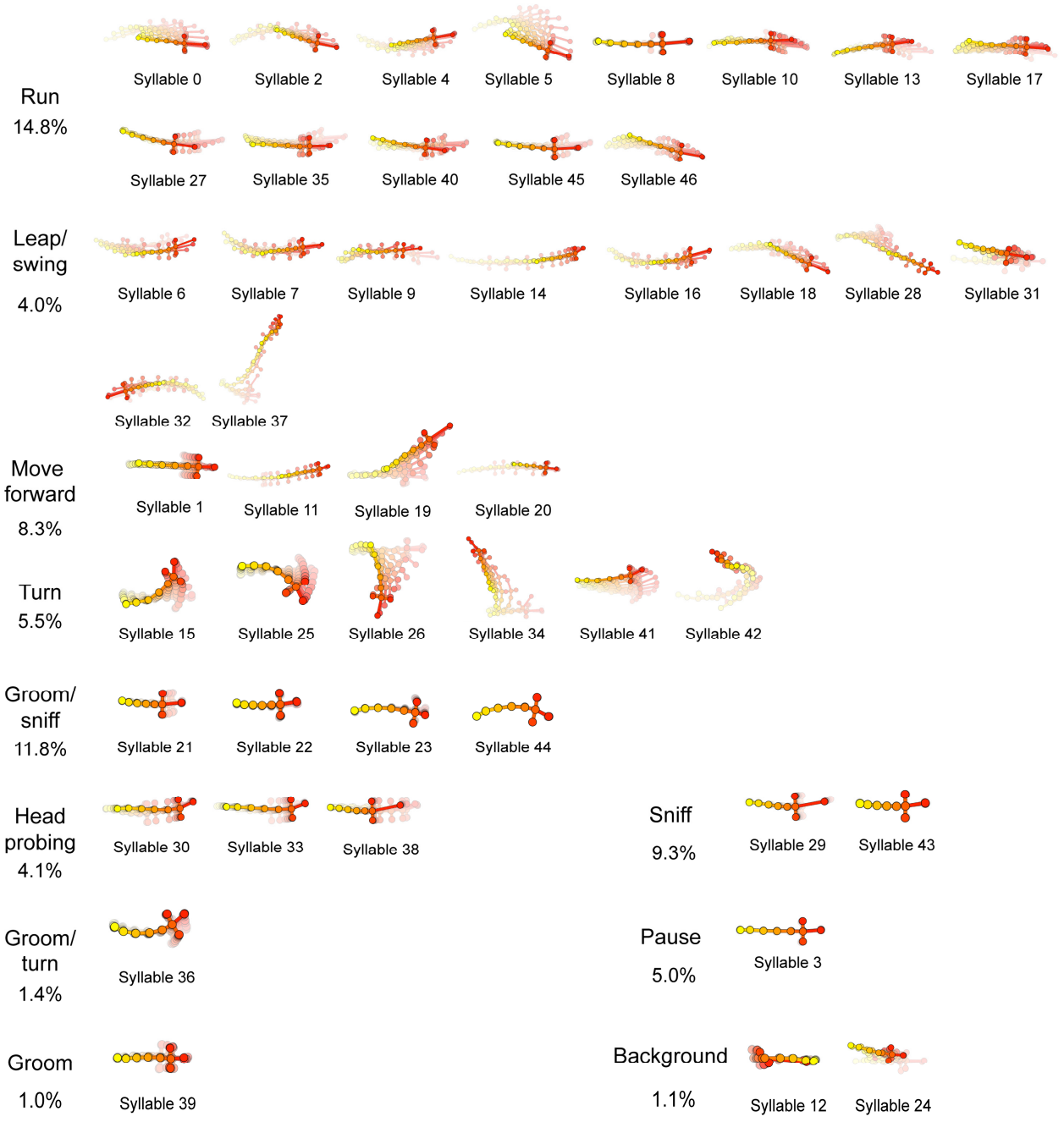

Supplemental Data Fig. 3. Keypoint-MoSeq trajectory plots of behavioral syllables. Syllables identified from keypoint coordinates by Keypoint-MoSeq were sorted into 11 categories by trained raters using grid movies generated for each syllable. The proportion of each syllable category is presented as a percentage. Rare syllables (minimum frequency < 0.5% but ≥ 0.01%) are not visually depicted but were included in the analysis.

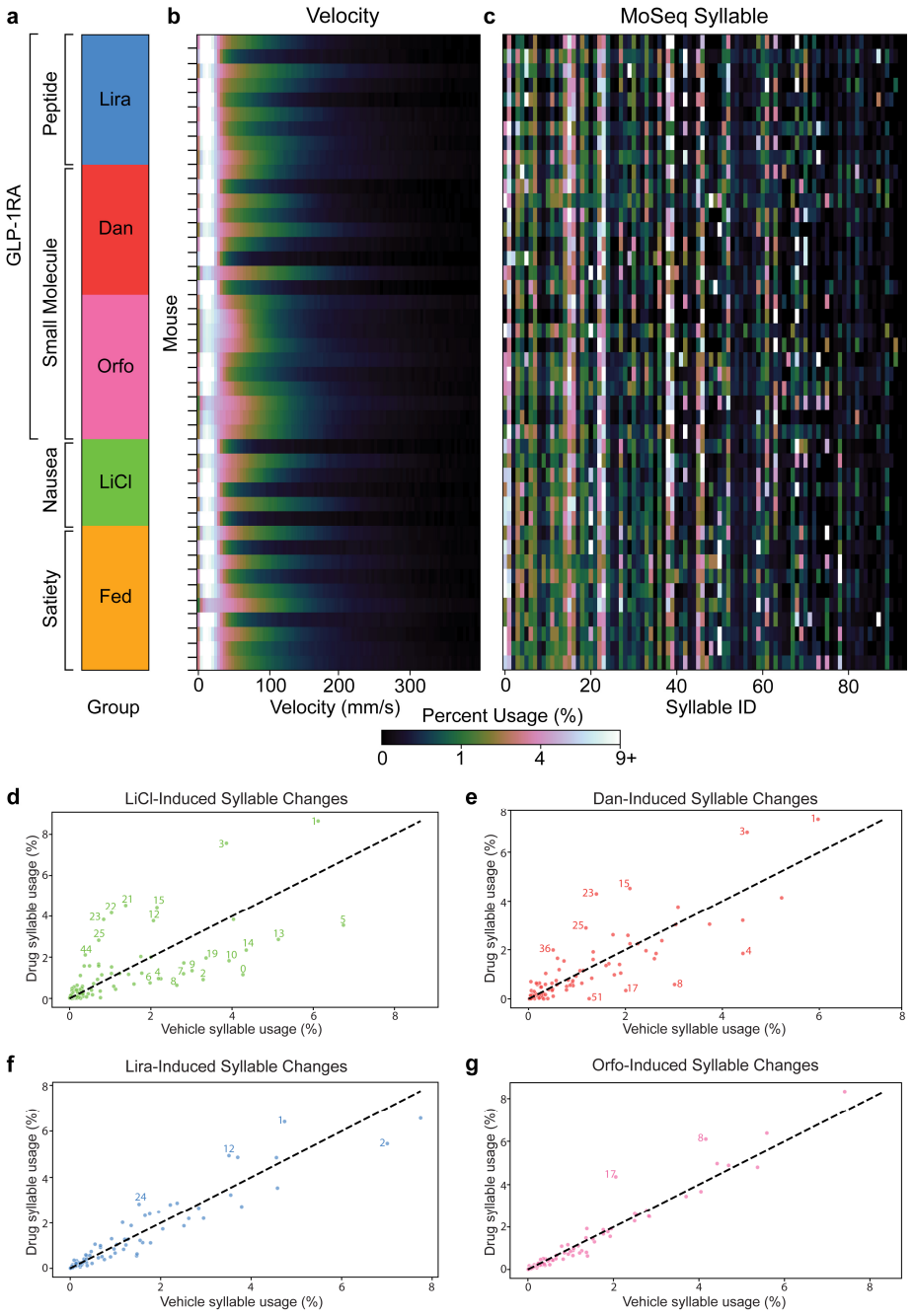

Supplemental Data Figure 4. Behavioral syllable usage and velocity. a–c, Each row represents an individual mouse assigned to one of five test conditions: liraglutide (Lira), danuglipron (Dan), orforglipron (Orfo), lithium chloride (LiCl), or pre-fed/satiated (Fed). **b**, Distribution of velocity usage over the two-hour home cage recording period. **c**, Percent usage of behavioral syllables identified by Keypoint-MoSeq. **d-g**, Change in usage of syllables across drug conditions relative to paired vehicle control. The top 10% of changes from baseline across all drug groups are labeled with their syllable identity number. Syllables above the dashed line show increased usage under drug conditions; those below show decreased usage for (**d**) LiCl, (**e**) Dan, (**f**) Lira, and (**g**) Orfo.

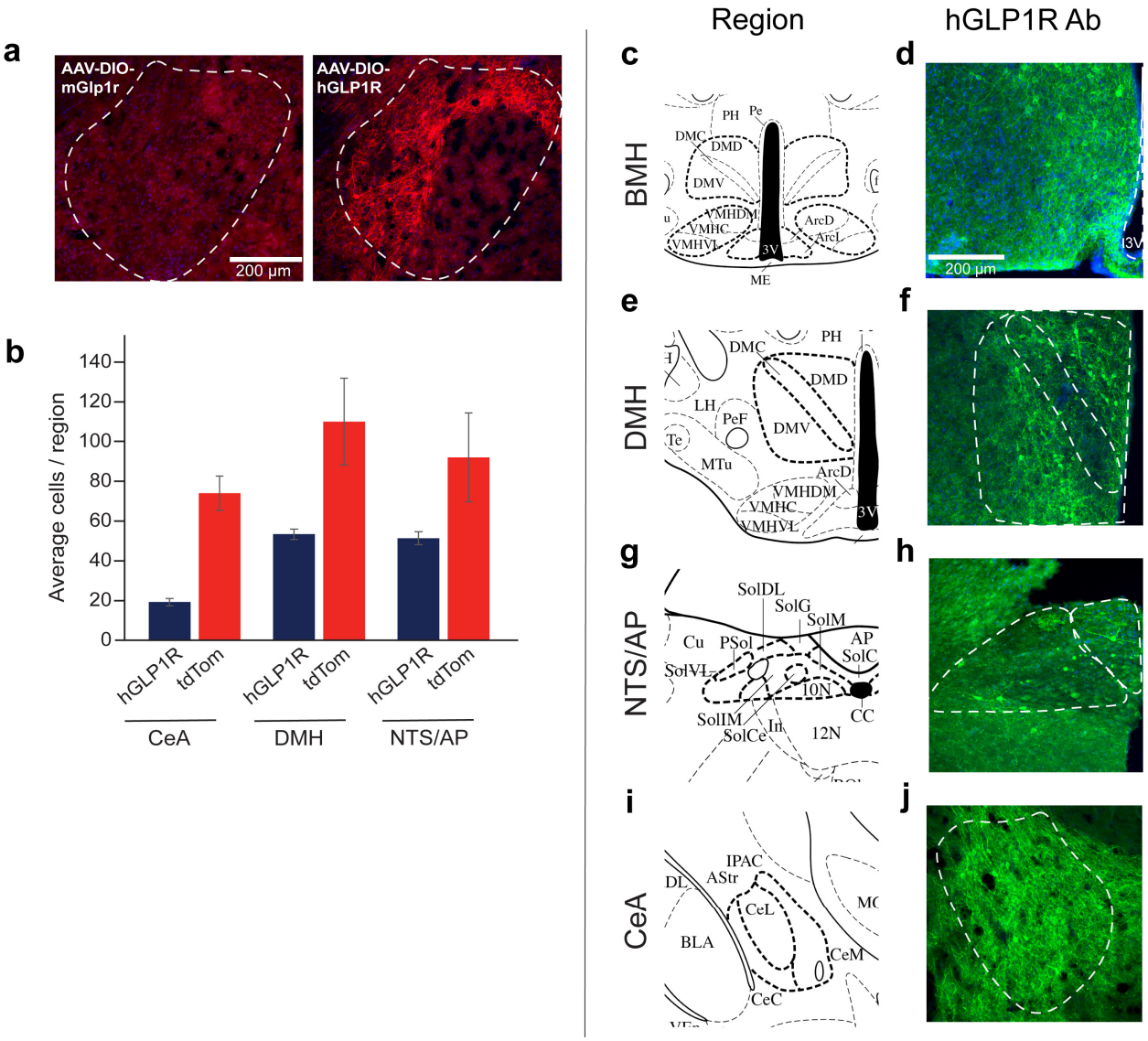

Supplemental Data Fig. 5. Validation of AAV-hSyn-DIO-hGLP1R virus. a, Validation of human GLP1R (hGLP1R; red) expression in the CeA of Glp1r-Cre mice injected with AAV-DIO-hGLP1R (right). hGLP1R protein expression is absent in Glp1r-Cre mice injected with AAV-DIO-mGlp1r in the CeA (left). Scale bar = 200 µm. **b**, Quantification of hGLP1R+ cells and average number of Glp1r+ cells (measured in Glp1r-Cre;tdTomato mice) in the CeA, DMH, or NTS/AP per section. Sample sizes per section: CeA hGLP1R *n* = 23, tdTomato *n* = 3; DMH hGLP1R *n* = 18, tdTomato *n* = 3; NTS/AP hGLP1R *n* = 15, tdTomato *n* = 6. **c-j,** Fluorescent microscopy images of the brain regions stereotaxically injected with AAV-DIO-hGLP1R. Images from Allen Brain Atlas, with regions of interest in bold and hGLP1R antibody staining (green) in the (**c,d**) basomedial hypothalamus (BMH), (**e,f**) DMH, (**g,h**) NTS/AP, or (**i,j**) CeA. Scale bars = 200 µm. Data are presented as mean ± SEM.

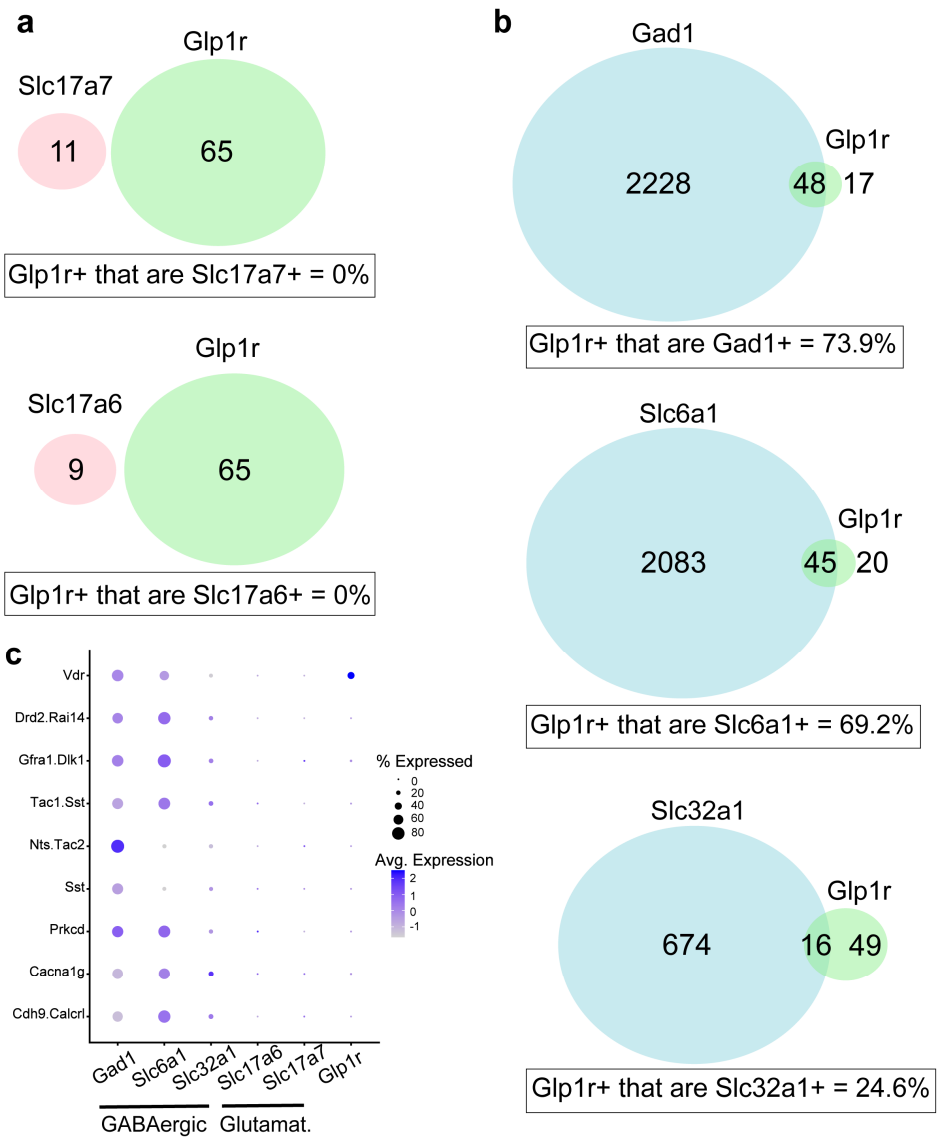

Supplemental Data Fig. 6. Transcriptomic profiling of CeA^{Glp1r} neurons. a-b, Coexpression analysis of Glp1r mRNA and glutamatergic markers (Slc17a7 and Slc17a6) and Glp1r and GABAergic markers (Gad1, Slc6a1, and Slc32a1). **c**, Dotplot showing Glp1r is expressed in the Vdr cluster that contains GABAergic markers. The transcriptomic analyses confirm that CeA^{Glp1r} neurons are GABAergic[39].

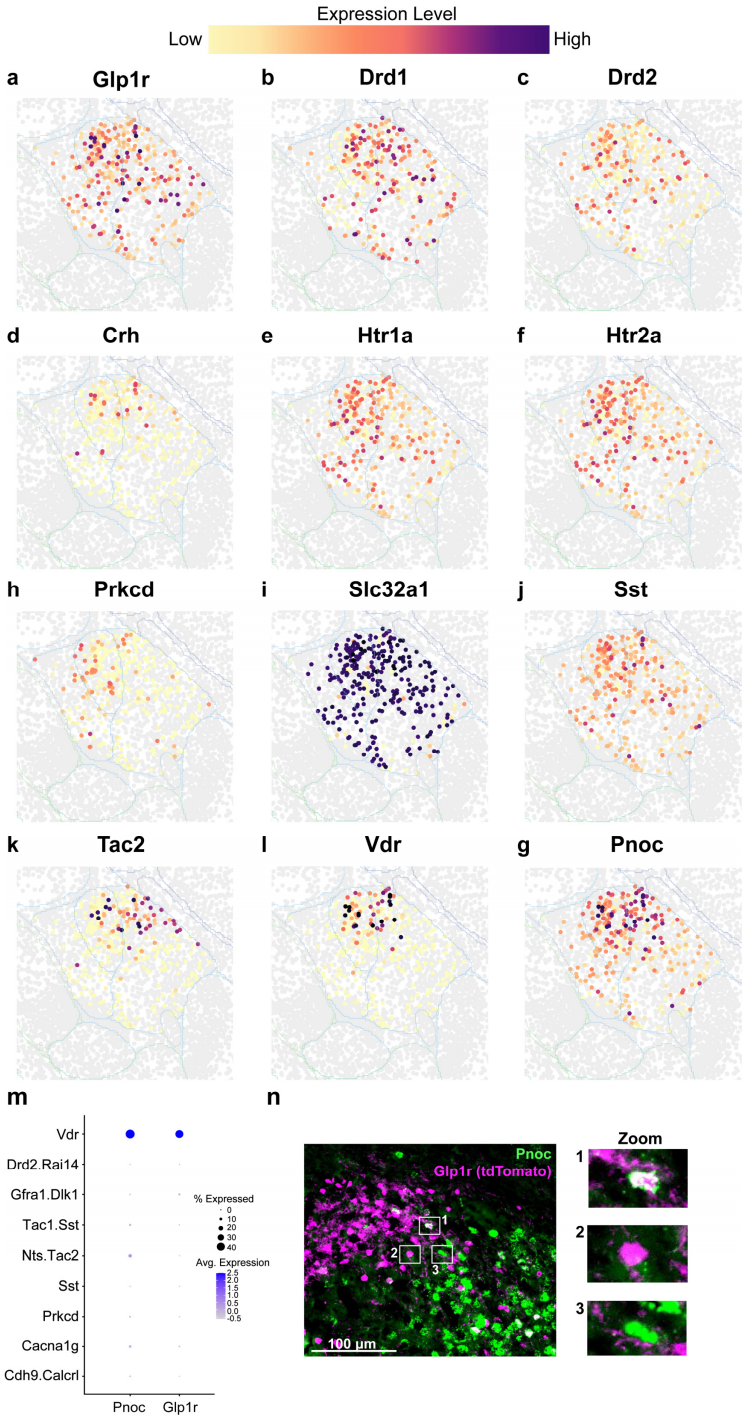

Supplemental Data Fig. 7. CeA *Glp1r* and *Pnoc* spatial expression analysis. (**a–l**) Representative MERFISH images from the Allen Brain Atlas of 12 marker transcripts in the CeA, showing relative expression levels from low (yellow) to high (purple)[40]. **m**, Dotplot showing *Glp1r* and *Pnoc* are expressed in the Vdr cluster[39]. **n**, Representative image for *Pnoc* RNAscope staining (green) and tdTomato protein expression (magenta) demonstrating some but not total overlap (white) between cell types in the CeA of Glp1r-Cre;TdTomato mice (29.9% overlap ± 3.8, *n* = 3 mice).

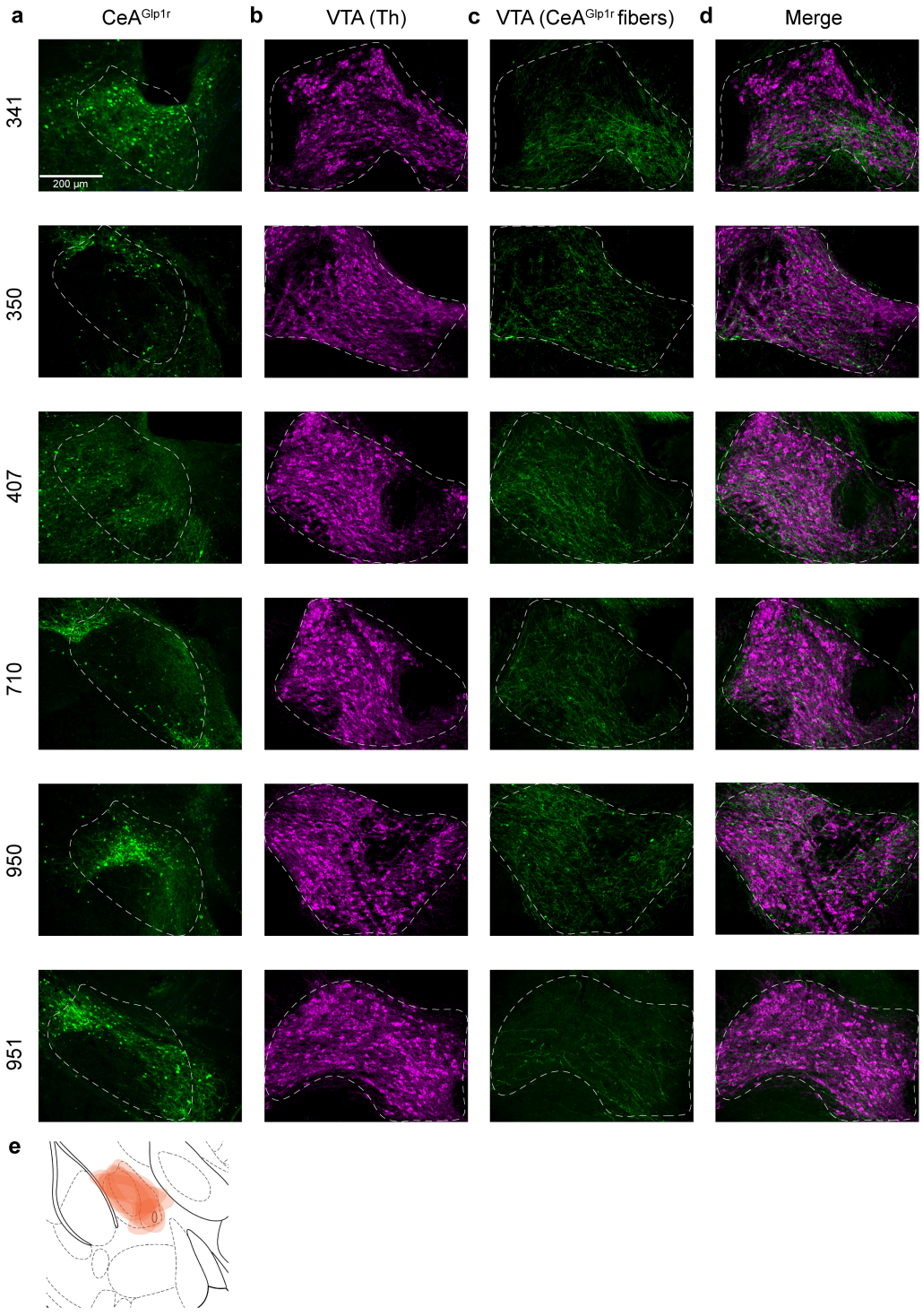

Supplemental Data Fig. 8. Validation of CeA^{Glp1r} targeting and VTA innervation. a, Representative images of AAV-DIO-ChR2-eYFP expression targeted to the CeA of Glp1r-Cre mice (green; *n* = 6). **b**, Tyrosine hydroxylase (Th) expression in the VTA (magenta). **c**, Axon fiber projections from CeA^{Glp1r} neurons into the VTA, and **d**, colocalization of Th with CeA^{Glp1r} fibers in the VTA. **e**, Traces of superimposed AAV-DIO-ChR2-eYFP injection targeting per mouse, collapsed on the Allen Brain Atlas figure.

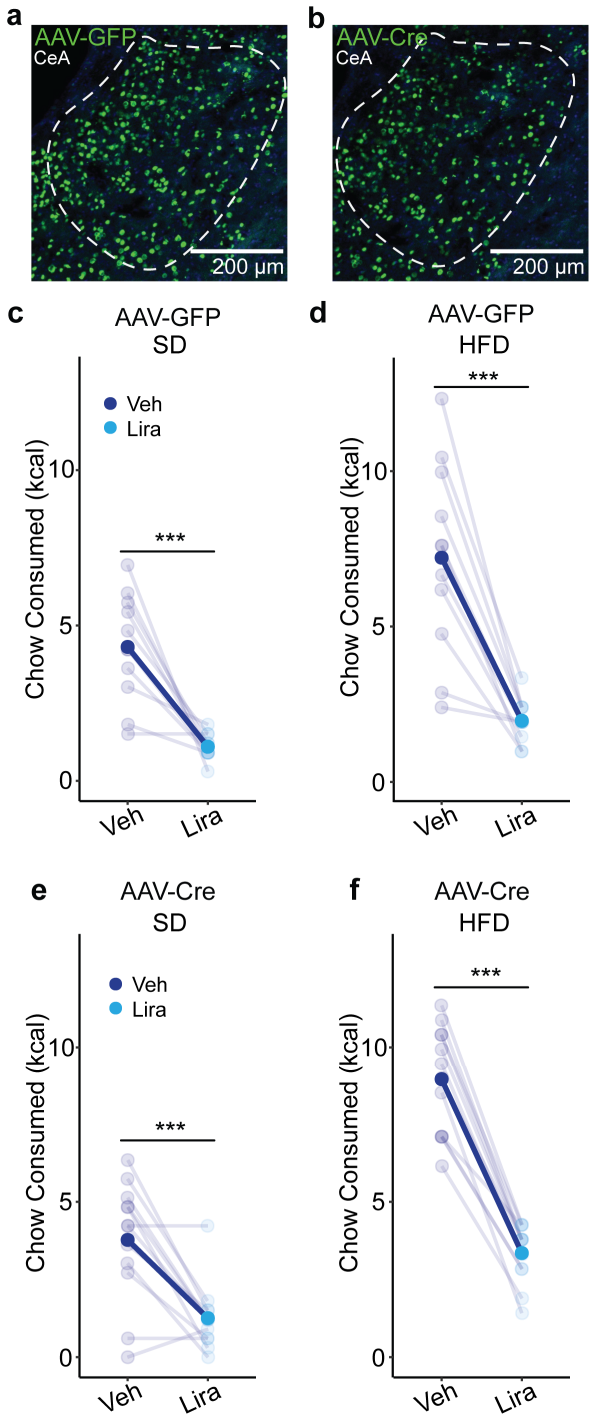

Supplemental Data Figure 9. Glp1r$^{flox/flox}$ AAV-Cre or AAV-GFP food intake. a-b, Validation of AAV-GFP (**a**) or AAV-Cre (**b**) targeting the CeA of Glp1r$^{flox/flox}$ mice. **c-d**, SD (**c**) and HFD (**d**) chow consumption 4 hours after injection of vehicle (Veh) or liraglutide (Lira) in AAV-GFP expressing mice. (n = 11, Paired t-test, ***P<0.001). **e-f**, SD (**e**) and HFD (**f**) chow consumption 4 hours after injection of Veh or Lira in AAV-Cre expressing mice. (n = 12, Paired t-test, ***P<0.001). Data are represented as means ± SEM.